Cellular Signalling 58 (2019) 65–78

Contents lists available at ScienceDirect

Cellular Signalling

journal homepage: www.elsevier.com/locate/cellsig

Fibulin-4 deficiency differentially affects cytoskeleton structure and dynamics as well as TGFβ signaling

Joyce Burger[a,b], Nicole van Vliet[a], Paula van Heijningen[a], Heena Kumra[c], Gert-Jan Kremers[d], Maria Alves[b], Gert van Cappellen[d], Hiromi Yanagisawa[e], Dieter P. Reinhardt[c,f], Roland Kanaar[a,g], Ingrid van der Pluijm[a,h], Jeroen Essers[a,h,i,*]

[a] Department of Molecular Genetics, Erasmus University Medical Center, Rotterdam, the Netherlands
[b] Department of Clinical Genetics, Erasmus University Medical Center, Rotterdam, the Netherlands
[c] Faculty of Medicine, Department of Anatomy and Cell Biology, McGill University, Montreal, Quebec, Canada
[d] Erasmus Optical Imaging Centre, Department of Pathology, Erasmus University Medical Center, Rotterdam, the Netherlands
[e] Life Science Center for Survival Dynamics, Tsukuba Advanced Research Alliance (TARA), University of Tsukuba, Tsukuba, Japan
[f] Faculty of Dentistry, McGill University, Montreal, Quebec, Canada
[g] Oncode Institute, Erasmus University Medical Center, Rotterdam, the Netherlands
[h] Department of Vascular Surgery, Erasmus University Medical Center, Rotterdam, the Netherlands
[i] Department of Radiation Oncology, Erasmus University Medical Center, Rotterdam, the Netherlands

ARTICLE INFO

Keywords:
Aneurysm
Molecular biology
TGFβ signaling
Cytoskeleton dynamics

ABSTRACT

Fibulin-4 is an extracellular matrix (ECM) protein essential for elastogenesis and mutations in this protein lead to aneurysm formation. In this study, we isolated vascular smooth muscle cells (VSMCs) from mice with reduced fibulin-4 protein expression (Fibulin-$4^{R/R}$) and from mice with a smooth muscle cell specific deletion of the Fibulin-4 gene (Fibulin-$4^{f/-}$/SM22Cre^{+}). We subsequently analyzed and compared the molecular consequences of reduced Fibulin-4 expression versus total ablation of Fibulin-4 expression with regard to effects on the SMC specific contractile machinery, cellular migration and TGFβ signaling.

Analysis of the cytoskeleton showed that while Fibulin-$4^{f/-}$/SM22Cre^{+} VSMCs lack smooth muscle actin (SMA) fibers, Fibulin-$4^{R/R}$ VSMCs were able to form SMA fibers. Furthermore, Fibulin-$4^{f/-}$/SM22Cre^{+} VSMCs showed a decreased pCofilin to Cofilin ratio, suggesting increased actin depolymerization, while Fibulin-$4^{R/R}$ VSMCs did not display this decrease. Yet, both Fibulin-4 mutant VSMCs showed decreased migration. We found increased activation of TGFβ signaling in Fibulin-$4^{R/R}$ VSMCs. However, TGFβ signaling was not increased in Fibulin-$4^{f/-}$/SM22Cre^{+} VSMCs.

From these results we conclude that both reduction and absence of Fibulin-4 leads to structural and functional impairment of the SMA cytoskeleton. However, while reduced levels of Fibulin-4 result in increased TGFβ activation, complete absence of Fibulin-4 does not result in increased TGFβ activation. Since both mouse models show thoracic aortic aneurysm formation, we conclude that not only hampered TGFβ signaling, but also SMA cytoskeleton dynamics play an important role in aortic aneurysmal disease.

1. Introduction

Aortic aneurysms are dilations of the aorta caused by a general weakening of the aortic wall. Patients affected by such dilations have a high risk of mortality upon rupture. Approximately 1–2% of all deaths in the western world are caused by aortic aneurysms and dissections [1]. The aortic wall consists of three layers, the intima, the media and the adventitia. The medial layer of the aortic wall contains the elastic laminae interspaced by vascular smooth muscle cells (VSMCs) and is important for the elasticity and contractility of the ascending aorta.

Abbreviations: ECM, Extracellular matrix; Fibulin-4^{R}, Mouse carrying Fibulin-4 mutant allele with reduced Fibulin-4 expression; Fibulin-4^{+}, Mouse carrying wildtype allele; Fibulin-4^{f}, Mouse carrying floxed Fibulin-4 allele that can be deleted by Cre recombinase; Fibulin-4^{-}, Mouse with Fibulin-4 knock-out; SM22 Cre^{+}, Mouse expressing Cre recombinase under SM22 promoter, Smooth muscle cell specific; SMA, Smooth muscle actin, smooth muscle cell specific form of actin; TGFβ, Transforming growth factor β; VSMC, Vascular smooth muscle cell

* Corresponding author at: Erasmus Medical Center, Room Ee702b, Wytemaweg 80, 3015 CN Rotterdam, POB 2040, 3000 CA Rotterdam, the Netherlands.
E-mail address: j.essers@erasmusmc.nl (J. Essers).

https://doi.org/10.1016/j.cellsig.2019.02.008
Received 16 November 2018; Received in revised form 28 February 2019; Accepted 28 February 2019
Available online 04 March 2019

During aneurysm formation the medial layer of the aorta is characterized by elastin layer fragmentation, loss of VSMCs and deposition of excess of extracellular matrix (ECM) material. These processes weaken the aortic wall and increase the risk of rupture [1,2].

Multiple genes have been identified to cause aneurysm formation when mutated. Mutations in the extracellular matrix protein fibrillin-1 (FBN1) lead to Marfan syndrome [3]. Mutations in proteins implicated in TGFβ signaling, such as TGFβ receptor 1 and 2 (TGFβR1 and TGFβR2) as well as SMAD3, lead to Loeys-Dietz syndrome characterized by aneurysm formation [4–8]. In addition, contractile or cytoskeletal protein mutations, such as α-smooth muscle actin (ACTA2) and myosin heavy chain 11 (MYH11) have been identified as causal genes for aneurysm formation [9–12]. Although these proteins are localized in different topological compartments, they most likely cooperate at a mechanistic molecular level and collectively play a role in aneurysm formation. We hypothesize that reduced presence or complete absence of the extracellular matrix protein fibulin-4 could influence cytoskeleton structure and dynamics since cell-ECM contact is mediated by transmembrane cell adhesion receptors, such as integrins, that interact with extracellular matrix proteins as well as a number of cytoplasmic adaptor proteins that interact with the actin cytoskeleton or function in signal transduction.

Fibulin-4 is an ECM protein that is essential for elastogenesis and is responsible for the recruitment of lysyl oxidase [13]. Lysyl oxidase is required for proper crosslinking of the elastin precursor tropoelastin to form mature elastic laminae [14]. These elastic laminae are of importance for the elasticity of the aorta and for deposition of latent TGFβ complexes [15]. When fibulin-4 is absent or unable to recruit lysyl oxidase, tropoelastin is not properly crosslinked. This leads to irregular elastic laminae that have a fragmented appearance [16]. *EFEMP2* (*Fibulin-4*) mutations in patients lead to cutis laxa, an autosomal recessive disease that is characterized by non-elastic and loose skin, aneurysms and tortuosity of the large arteries [17–19]. Cutis laxa patients have either reduced fibulin-4 protein levels in tissues, or reduced binding of fibulin-4 to its targets. Furthermore, increased TGFβ signaling is detected in these patients [17,20].

Different mouse models have been generated to investigate the role of Fibulin-4 in aneurysm formation. While complete absence of Fibulin-4 is perinatal lethal, hypomorphic mice with 4-fold reduced expression levels (Fibulin-$4^{R/R}$, in which 'R' indicates the reduced expression allele) are viable [21,22]. Like cutis laxa patients, Fibulin-$4^{R/R}$ mice show aortic aneurysm formation, elastic laminae fragmentation and increased TGFβ signaling [22,23]. In addition, VSMC-specific knock-out mice for Fibulin-4 (Fibulin-$4^{f/-}$/SM22Cre^{+}) also develop aneurysms exclusively in the ascending aorta [24]. This mouse model has previously been used to determine the role of fibulin-4 in aortic development, and is instrumental to determine the role of fibulin-4 in aneurysm formation and VSMC function.

In this study we compared VSMCs isolated from aortas of Fibulin-$4^{R/R}$ and Fibulin-$4^{f/-}$/SM22Cre^{+} mice to analyze the consequences of diminished and completely ablated Fibulin-4 expression on cytoskeleton dynamics, cell movement and TGFβ signaling.

2. Materials and methods

2.1. Mice

Fibulin-$4^{R/R}$ and Fibulin-$4^{f/-}$/SM22Cre^{+} were generated and described previously [22,24]. Animals were housed at the Animal Resource Centre (Erasmus University Medical Centre), which operates in compliance with the "Animal Welfare Act" of the Dutch government, using the "Guide for the Care and Use of Laboratory Animals" as its standard. As required by Dutch law, formal permission to generate and use genetically modified animals was obtained from the responsible local and national authorities. An independent Animal Ethics Committee consulted by Erasmus Medical Center (Stichting DEC Consult) approved these studies (permit number 140-12-05), in accordance with national and international guidelines. Animals were sacrificed by CO_2 inhalation, unless stated otherwise. This study conforms to the guidelines from Directive 2010/63/EU of the European Parliament on the protection of animals used for scientific purposes or the NIH guidelines.

2.2. VSMC isolation and cell culture

Mice (at an age of 100 days) were euthanized and autopsied according to standard protocols. Primary VSMCs from the thoracic aorta were isolated according to the collagenase digestion method of Proudfoot and Shanahan [25]. Each cell line was derived from a single aorta. Fibulin-$4^{+/+}$ and Fibulin-$4^{f/+}$/SM22Cre^{+} VSMCs were used as controls, in which Fibulin-$4^{f/+}$/SM22Cre^{+} VSMCs also served as controls for the potential toxic effects of Cre recombinase. Due to differences in the genetic background of the mice (Fibulin-$4^{+/+}$ and Fibulin-$4^{R/R}$: C57Bl/6, Fibulin-$4^{f/+}$/SM22Cre^{+} and Fibulin-$4^{f/-}$/SM22Cre^{+}: C57Bl/6 and SJL), Fibulin-$4^{f/+}$/SM22Cre^{+} VSMCs will be used as a primary control for Fibulin-$4^{f/-}$/SM22Cre^{+} VSMCs. Fibulin-$4^{f/+}$/SM22Cre^{+} VSMCs show a decrease in Fibulin-4 expression compared to Fibulin-$4^{+/+}$ VSMCs (Fig. 1A), due to the deletion of one floxed allele by Cre recombinase. When experiments were performed simultaneously, we depicted all four genotypes (Fibulin-$4^{+/+}$, Fibulin-$4^{R/R}$, Fibulin-$4^{f/+}$/SM22Cre^{+} and Fibulin-$4^{f/-}$/SM22Cre^{+}) together. In the figures, Fibulin-$4^{f/+}$/SM22Cre^{+} and Fibulin-$4^{f/-}$/SM22Cre^{+} VSMCs are referred to as Fibulin-$4^{f/+}$ and Fibulin-$4^{f/-}$, respectively. Unless otherwise specified two cell lines were used per genotype. Primary VSMCs were cultured on gelatinized dishes in Dulbecco's Modified Eagle's Medium (DMEM) (Lonza BioWhittaker) supplemented with 1% penicillin-streptomycin (PS) and 10% fetal calf serum (FCS).

2.3. RNA isolation and real-time PCR

RNA from VSMCs was isolated with the RNeasy mini kit (Qiagen). cDNA was made with iScript cDNA synthesis kit (Biorad) according to manufacturing protocol. Q-PCR was performed with 200 nM forward and reverse primers and iQ™ SYBR® Green Supermix (Biorad) on the CFX96 system (Biorad); denaturation at 95 °C for 3 min, 40 cycles denaturation at 95 °C for 15 s, annealing/extension at 55 °C for 30 s. *B2M* and *β-actin* were used as reference genes and gave similar expression. Data is shown with *B2M* as a reference gene. Relative gene expression levels were determined with the comparative Ct (also referred to as ΔΔCt) method according to the MIQE guidelines. See Table 1 for primers used. Number of replicates is specified in the figure legends.

2.4. Western blotting

Western blot analysis was performed to determine protein amounts in extracts of Fibulin-$4^{f/-}$/SM22Cre^{+} and Fibulin-$4^{R/R}$ VSMCs compared to their controls. Cultured VSMCs were scraped in PBS supplemented with protease inhibitor cocktail (1:100, 11,836,145,001, Roche applied science) and phosphatase inhibitor cocktail (1:100, P0044, Sigma) and lysed in an equal volume of 2× Laemmli buffer (4% SDS, 20% glycerol, 120 mM Tris pH 6,8) supplemented with protease inhibitor cocktail and phosphatase inhibitor. Lysates first cleared from large DNA by passing through a 25G needle and then heated to 65 °C for 10 min. Protein concentrations were measured with the Lowry protein

Table 1
Primer sequences used for real-time PCR.

Gene	Fw sequence	Rev sequence
Fibulin-4	GGGTTATTTGTGTCTGCCTCG	TGGTAGGAGCCAGGAAGGTT
B2M	CTCACACTGAATTCACCCCCA	GTCTCGATCCCAGTAGACGGT
β-actin	AGATCAAGATCATTGCTCCTCCTG	GGGTGTAAAACGCAGCTCAG

Table 2
Antibodies used for Western blot analysis.

Primary antibody	Predicted kDa	Dilution	Manufacturer	Catalog number
Mouse α-β actin IgG2b	43	1:500.000	Merck Millipore	MAB1501
Mouse α-SMA IgG2a	40	1:10.000	Abcam	Ab7817
Rabbit α-SM22 IgG	23	1:2000	Abcam	Ab14106
Rabbit α-Cofilin IgG	19	1:2000	Abcam	Ab11062-50
Rabbit α-pCofilin (Ser3) IgG	19	1:1000	Cell signaling	3313S
Rabbit α-SMAD2 IgG	60	1:1000	Cell signaling	5339S
Rabbit α-pSMAD2 IgG	55–60	1:400	Merck Millipore	04-953
Mouse α-β catenin IgG1	92	1:2000	BD Bioscience	610153

assay as described [26]. Equal amounts of protein (10 µg per sample) were separated for size by SDS-PAGE and then transferred to a PVDF membrane (1 h, 100 V, Immobilon) and blocked with either 3% milk or 5% BSA in PBS supplemented with 0.1% Tween-20 (1 h, room temperature). The primary antibody was incubated overnight at 4 °C (see Table 2 for primary antibodies). The membranes were washed 5 times with 0.1% Tween-20 in PBS and then incubated with horseradish peroxidase-conjugated secondary antibodies (1:2000, Jackson ImmunoResearch) for 1 h at room temperature. Bound secondary antibodies were detected with an Amersham Imager 600 (GE Healthcare Life Sciences) using chemiluminescence. Band intensity was quantified using Fiji image analyzing software [27]. Number of replicates is specified in the figure legends.

2.5. Immunofluorescence

For in situ visualization of actin fibers, α-SMA and paxillin, VSMCs were seeded on 0.01% collagen coated coverslips and allowed to attach for 48 h. VSMCs were fixed with 2% paraformaldehyde in PBS for 15 min. After fixation coverslips were washed with PBS with 0.1% Trition-X100 and blocked with PBS+ (PBS supplemented with 0.15% glycine and 0.5% bovine serum albumin) for 30 min. Primary antibodies were incubated overnight at 4 °C in PBS+, α-SMA (1:750, ab7871, Abcam) and Paxillin (1:400, ab32115, Abcam). Coverslips were washed with PBS with 0.1% trition-X100 and incubated shortly with PBS+ prior to incubation with the secondary antibody in PBS+ (1:1000, anti-mouse Alexa Fluor 488 and anti-rabbit Alexa Fluor 594, Molecular Probes) at RT for 1 h. After incubation the coverslips were mounted on glass slides with Vectashield supplemented with DAPI (H-1200, Vector laboratories) and sealed with nail polish. Images were recorded on a wide field epifluorescent microscope (Axio Imager D2, Zeiss).

2.6. Live cell imaging

VSMCs were seeded at a density of 10,000 cells/cm^2 on a 0.01% collagen coated coverslip. VSMCs were allowed to attach for 48 h prior to transfection with a Paxillin-EGFP construct (2 µg/6-well) using Lipofectamin 3000 (L3000-015, Thermo Fisher). Plasmid pPaxillin-EGFP encodes an Paxillin-EGFP fusion protein, consisting of the chicken (*Gallus gallus*) paxillin protein fused to EGFP through a 22 amino acid linker. Plasmid pPaxillin-EGFP was made by substituting the mTurquoise cDNA in plasmid pmTurquoise-Paxillin-22 (Addgene plasmid # 55573) for the EGFP cDNA from plasmid pEGFP-N1 (Clontech) as a BamH1/*Not*I DNA fragment. After 6 h, the transfection medium was replaced with regular medium and VSMCs were allowed to recover overnight. The medium was replaced with medium supplemented with 150 nM SiR-Actin (SC001, Cytoskeleton, Inc.) to label actin filaments. After 6 h the VSMCs were imaged overnight with a confocal laser scanning microscope, Leica SP5 microscope (Leica, Mannheim). Images were recorded every 10 min at three levels of the cell (base, middle and top, 1 µm separated from each other). Movement of the VSMCs was quantified by Fiji image analysis software. After delineating the maximum projection, VSMCs were manually tracked with MTrackJ [28]. Total length of the path was used for comparing the mean migration velocity of Fibulin-4$^{f/+}$, Fibulin-4$^{f/-}$, Fibulin-4$^{+/+}$ and Fibulin-4$^{R/R}$ VSMCs.

2.7. G-actin/F-actin in vivo assay

The ratio between filamentous actin and monomeric actin was determined with a G-actin/F-actin in vivo assay kit (BK037, Cytoskeleton, Inc.). Two days prior to the experiment, VSMCs were seeded on 0.01% collagen coated wells to reach an almost confluent density at the time of lysis. Manufacturer protocol was followed for the lysis and fractionation of the F- and G-actin, ultracentrifugation of the samples was performed at room temperature. Equal volumes of supernatant (G-actin) and pellet (F-actin) lysates (10 µl per sample) were run on 12% gels according to the above described Western blotting protocol. Analysis of the fractions was performed with Fiji image analysis software. Number of replicates is specified in the figure legends.

2.8. Immunofluorescence of extracellular matrix

ECM protein production by VSMCs was determined by immunofluorescence. VSMCs were seeded at 25,000 cells/well, except for Fibulin-4 staining that required a higher seeding density of 75,000 cells/well, in 8-well removable chamber slides and grown in DMEM supplemented with 10% heat-inactivated FCS and 1% PS for 7 days to allow ECM deposition. VSMCs were fixed with an ice-cold 70:30 methanol:acetone mixture for 5 min and washed with PBS. Coverslips were blocked for 1 h with PBS supplemented with 10% normal goat serum (X0907, Agilent). Primary antibodies (Table 3) were incubated overnight at 4 °C in PBS. Coverslips were washed three times with PBS for 5 min each prior to incubation with the secondary antibody for 1.5 h at room temperature (1:1000, anti-rabbit Alexa Fluor 594, Molecular Probes). Coverslips were washed and mounted to glass slides with Vectashield supplemented with DAPI (H-1200, Vector laboratories) and sealed with nail polish. Images were recorded on a wide field epifluorescent microscope (Axio Imager D2, Zeiss). Fibulin-4 images were

Table 3
Antibodies used for immunofluorescent staining of the ECM.

Primary antibody	Dilution	Manufacturer	Catalog number
Rabbit α-fibronectin IgG	1:80	Millipore	AB2033
Rabbit α-mouse fibrillin-1	1:1000	Generated in Reinhardt Lab	–
Rabbit α-mouse LTBP4	1:1000	Generated in Reinhardt Lab	–

recorded on a Axio Imager M2 epifluorescent microscope, Zeiss.

2.9. TGFβ reporter assay

Downstream activation of the TGFβ pathway was determined via a CAGA-MLP-luciferase promoter reporter construct [29]. This construct contains palindromic repeats of the SMAD3/SMAD4 binding site of the PAI-1 promoter and was shown to be sensitive to TGFβ [29]. VSMCs were seeded the day prior to transfection in gelatinized 24 well plates. Subconfluent cells were transfected with Lipofectamin 3000 according to the manufacturer protocol. A SV40-renilla construct (Addgene plasmid # 27163, [30]) was co-transfected to correct for transfection efficiency. After 6 h, the transfection medium was replaced with DMEM supplemented with 10% FCS and 1% PS. On the following day the VSMCs were serum starved for 2 h by DMEM supplemented with 0.2% FCS and 1% PS. The VSMCs were then treated overnight with serum starvation medium supplemented with 5 ng/ml TGFβ1 (4342-5, Biovision) or 10 μM SB43542 hydrate (S4317-5 mg, Sigma) or without stimulation. VSMCs were washed with PBS, lysed and luciferase activity was measured with the dual-luciferase kit (E1910, Promega) with the GloMax-multi detection system (Promega). Number of replicates is specified in the figure legends.

2.10. Statistical analysis

All experiments were performed in triplicate using three independent samples. Data were corrected for outliers with the Grubbs' test for outliers. Statistical analysis was performed with a non-parametric Mann-Whitney test. Significance was tested 2-tailed. A p-value < .05 was considered to indicate a significant difference between groups. In the figures $p < .05$ is show with *, $p < .01$ with $, $p < .001$ with ‡, and $p < .0001$ with #. Results are expressed as mean ± SD, real-time PCR results are expressed as geometric mean ± geometric SD. All analyses were performed using Graphpad, version 7.03.

3. Results

3.1. Fibulin-4 mutations affect the SMA cytoskeleton

To compare the consequences of complete Fibulin-4 deletion versus decreased expression of Fibulin-4, we isolated VSMCs from aortas of Fibulin-$4^{f/-}$/SM22Cre^{+} (VSMC-specific deletion of the Fibulin-4 gene) and Fibulin-$4^{R/R}$ (reduced expression of the Fibulin-4 gene) animals and their respective control littermates. First, *Fibulin-4* gene expression was determined in Fibulin-$4^{R/R}$, Fibulin-$4^{f/-}$/SM22Cre^{+}, Fibulin-$4^{+/+}$ and Fibulin-$4^{f/+}$/SM22Cre^{+} VSMCs. *Fibulin-4* expression in Fibulin-$4^{R/R}$ VSMCs is approximately 20% of the Fibulin-$4^{+/+}$ VSMCs (Fig. 1A). No *Fibulin-4* expression was detected in Fibulin-$4^{f/-}$/SM22Cre^{+} VSMCs while *Fibulin-4* gene expression was present in the control Fibulin-$4^{f/+}$/SM22Cre^{+} VSMCs, but significantly reduced to about 50% compared to Fibulin-$4^{+/+}$ (Fig. 1A).

Previously Huang et al. have shown that VSMC-specific deletion of *Fibulin-4* leads to decreased expression of ACTA2 in Fibulin-$4^{f/-}$/SM22Cre^{+} aortas, indicating that absence of Fibulin-4 impairs differentiation and proper SMA cytoskeleton formation [24]. To further analyze these isolated VSMCs, cells were stained for SMA and paxillin. SMA is a marker for the contractile, non-proliferative phenotype of adult VSMCs and paxillin is a multidomain adaptor localized at the interface between the plasma membrane and the actin cytoskeleton. The control VSMCs, Fibulin-$4^{f/+}$/SM22Cre^{+} and Fibulin-$4^{+/+}$ showed numerous SMA stress fibers spanning their cytoplasm (Fig. 1B). The well spread controls adhered to the surface with elongated focal contacts positive for paxillin, positioned at the end of the individual SMA fibers (Fig. 1C, top and bottom image). The arrows indicate the overlay between SMA fibers and the focal adhesions in yellow. In Fibulin-$4^{f/-}$/SM22Cre^{+} VSMCs SMA stress fibers were not present and paxillin staining identified small rounded podosome-like structures instead of the elongated structures observed in control VSMCs. This was further confirmed in higher magnification images (Fig. 1C and D). The Fibulin-$4^{R/R}$ VSMC did show SMA stress fibers, however, these fibers were not as distinct as in control VSMCs. Yet, paxillin did localize to the ends of SMA fibers and also formed elongated structures as was seen in the control VSMCs. Western blotting on whole cell lysates showed presence of SMA in both the Fibulin-$4^{f/+}$/SM22Cre^{+} and the Fibulin-$4^{+/+}$ control VSMCs. Compared to the Fibulin-$4^{f/+}$/SM22Cre^{+} and Fibulin-$4^{+/+}$ VSMCs SMA expression was significantly decreased in Fibulin-$4^{f/-}$/SM22Cre^{+} (Fig. 1E and F, $p < .0001$). In contrast, Fibulin-$4^{R/R}$ VSMCs whole cell lysates showed an increase in SMA protein levels compared to Fibulin-$4^{+/+}$ whole cell lysates (Fig. 1E and F, $p < .0001$). Similarly, Fibulin-$4^{f/+}$/SM22Cre^{+} VSMCs with 50% Fibulin-4 gene expression showed a significant increase in SMA protein compared to Fibulin-$4^{+/+}$ VSMCs (Fig. 1E and F, $p < .0001$).

These results show that complete absence of Fibulin-4 leads to loss of SMA stress fibers, while reduced levels of Fibulin-4 can support SMA fiber formation. However, this fiber formation appears affected, even though the total amount of SMA protein is increased in Fibulin-$4^{R/R}$ VSMCs. Furthermore, absence of Fibulin-4 in the Fibulin-$4^{f/-}$/SM22Cre^{+} VSMCs also leads to an aberrant, podosome-like, appearance of the focal adhesion structures.

3.2. Actin dynamics are differentially affected by Fibulin-4 mutations

The actin cytoskeleton is a dynamic structure in which actin monomers are continuously polymerized and depolymerized. The lack of SMA fibers in Fibulin-$4^{f/-}$/SM22Cre^{+} VSMCs suggests less polymerization of actin monomers into actin fibers or, alternatively, increased depolymerization in Fibulin-$4^{f/-}$/SM22Cre^{+} VSMCs. Previously, alteration in actin depolymerization in Fibulin-$4^{f/-}$/SM22Cre^{+} aortic tissue lysates has been linked to decrease in phosphorylated cofilin to total cofilin ratio and the restoration of cofilin phosphorylation prevented aneurysm formation [31]. This shift increases activity of cofilin leading to increased depolymerization of the actin fibers. In addition, SM22, an actin crosslinking protein and VSMC differentiation marker, is decreased in Fibulin-$4^{f/-}$/SM22Cre^{+} aortic tissue lysates, suggesting that the VSMCs are not fully differentiated into mature VSMCs when Fibulin-4 is completely absent [31–33].

To determine if actin is still polymerized in mature actin filaments in Fibulin-$4^{f/-}$/SM22Cre^{+} VSMCs and Fibulin-$4^{R/R}$ VSMCs, we performed an F-/G-actin fractionation by which the ratio of polymerized versus free actin monomers can be determined (Fig. 2A and B). This fractionation revealed a decrease in F-actin levels over G-actin levels in Fibulin-$4^{f/-}$/SM22Cre^{+} VSMCs compared to control Fibulin-$4^{f/+}$/SM22Cre^{+} VSMCs (Fig. 2B, $p < .01$). No significant difference in F-actin/G-actin fraction was found in Fibulin-$4^{R/R}$ VSMCs compared to Fibulin-$4^{+/+}$ VSMCs (Fig. 2B). The F-actin/G-actin fraction of Fibulin-$4^{f/-}$/SM22Cre^{+} VSMCs was also significantly decreased compared to both Fibulin-$4^{+/+}$ and Fibulin-$4^{R/R}$ VSMCs (Fig. 2B, $p < .05$).

The ratio of phosphorylated cofilin to cofilin was determined by western blot analysis to analyze the amount of inactive to active cofilin, respectively. We observed a decrease in the phosphorylated cofilin to cofilin ratio in Fibulin-$4^{f/-}$/SM22Cre^{+} VSMCs compared to Fibulin-$4^{+/+}$ VSMCs (Fig. 2C and D, $p < .01$). This shift in ratio towards more active cofilin leads to increased depolymerization of actin fibers in Fibulin-$4^{f/-}$/SM22Cre^{+} VSMCs. In Fibulin-$4^{R/R}$ VSMCs the ratio of phosphorylated cofilin to cofilin was comparable to Fibulin-$4^{+/+}$ VSMCs (Fig. 2C and D). When comparing the ratio of phosphorylated cofilin to cofilin in Fibulin-$4^{f/+}$/SM22Cre^{+} VSMCs no difference was found compared to Fibulin-$4^{+/+}$ VSMCs (Fig. 2C and D).

Western blot analysis for SM22 protein levels was performed to assess the differentiation status of the VSMCs and the actin crosslinking potential in Fibulin-$4^{f/-}$/SM22Cre^{+} and Fibulin-$4^{R/R}$ VSMCs. SM22

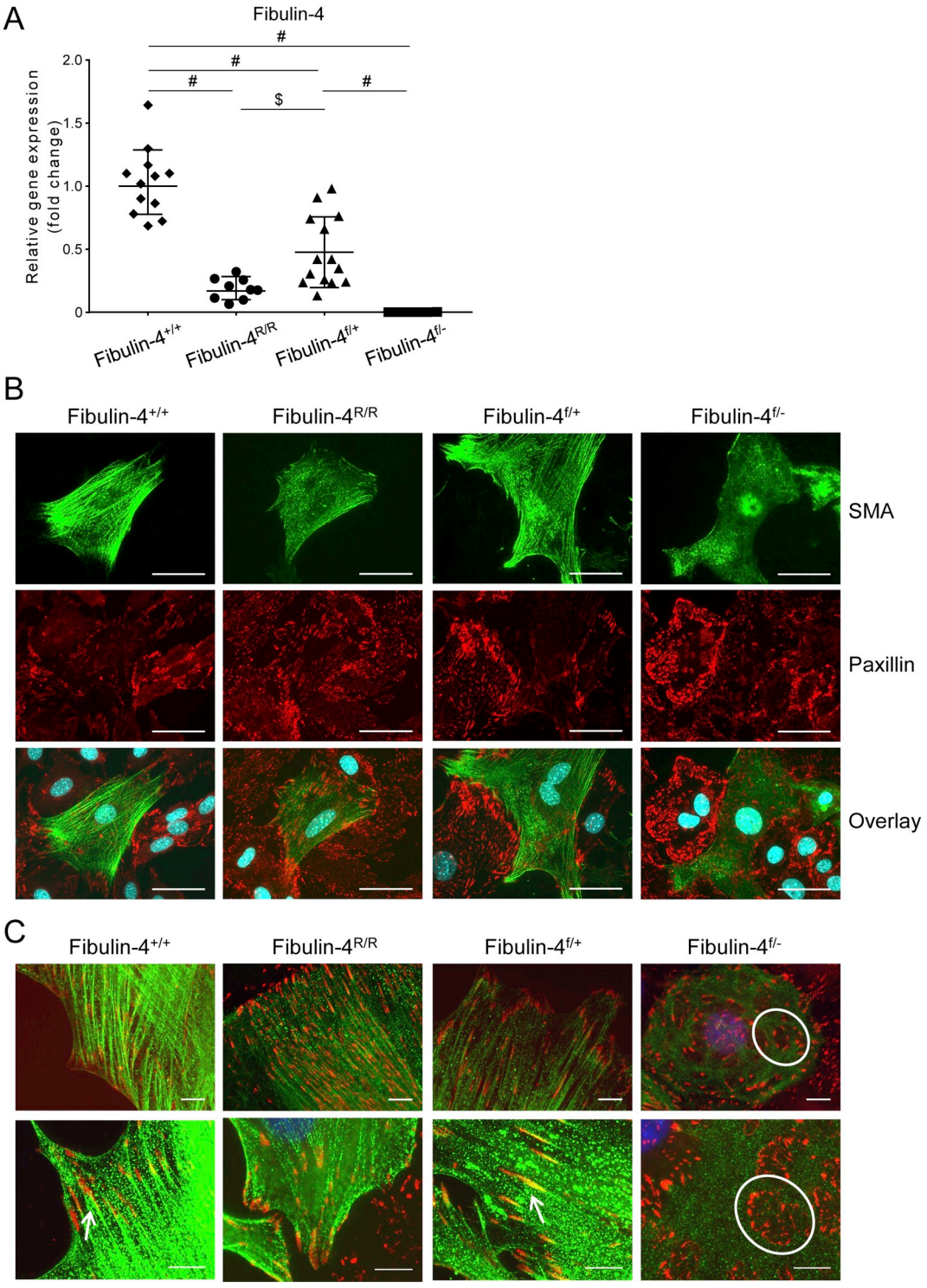

Fig. 1. Fibulin-4 is needed for SMA fiber formation. A) Relative gene expression of *Fibulin-4* in Fibulin-$4^{+/+}$, Fibulin-$4^{R/R}$, Fibulin-$4^{f/+}$ and Fibulin-$4^{f/-}$ VSMCs. Data is shown for $n = 3$–7 lysates in 2 independent experiments. B) Immunofluorescent staining of SMA in green and paxillin in red. Scale bar represents 50 μm. C) Close up of paxillin and SMA staining. Paxillin forms elongated structures that localize to the tips of SMA fibers in Fibulin-$4^{+/+}$ and Fibulin-$4^{f/+}$ VSMCs (arrow indicates an example of overlap between SMA and paxillin). In Fibulin-$4^{f/-}$ VSMCs paxillin did not localize to SMA fibers and formed small rounded podosome-like structures (one example shown in circle). Scale bar represents 10 μm. D) Further close-up of actin fibers and paxillin overlay in Fibulin-$4^{f/+}$ and podosome-like structures of paxillin in Fibulin-$4^{f/-}$ VSMC. Scale bar represent 10 μm. E) Western blots detecting SMA in Fibulin-$4^{+/+}$, Fibulin-$4^{R/R}$, Fibulin-$4^{f/+}$ and Fibulin-$4^{f/-}$ VSMC protein extracts. β-catenin levels serve as a loading control. F) Quantification of SMA levels as shown in panel E, respectively. Data is shown for $n = 7$–8 lysates in 3 independent experiments. Bars represent mean ± SD. Mann-Whitney test. $\$ p < .01$, $\# p < .0001$.

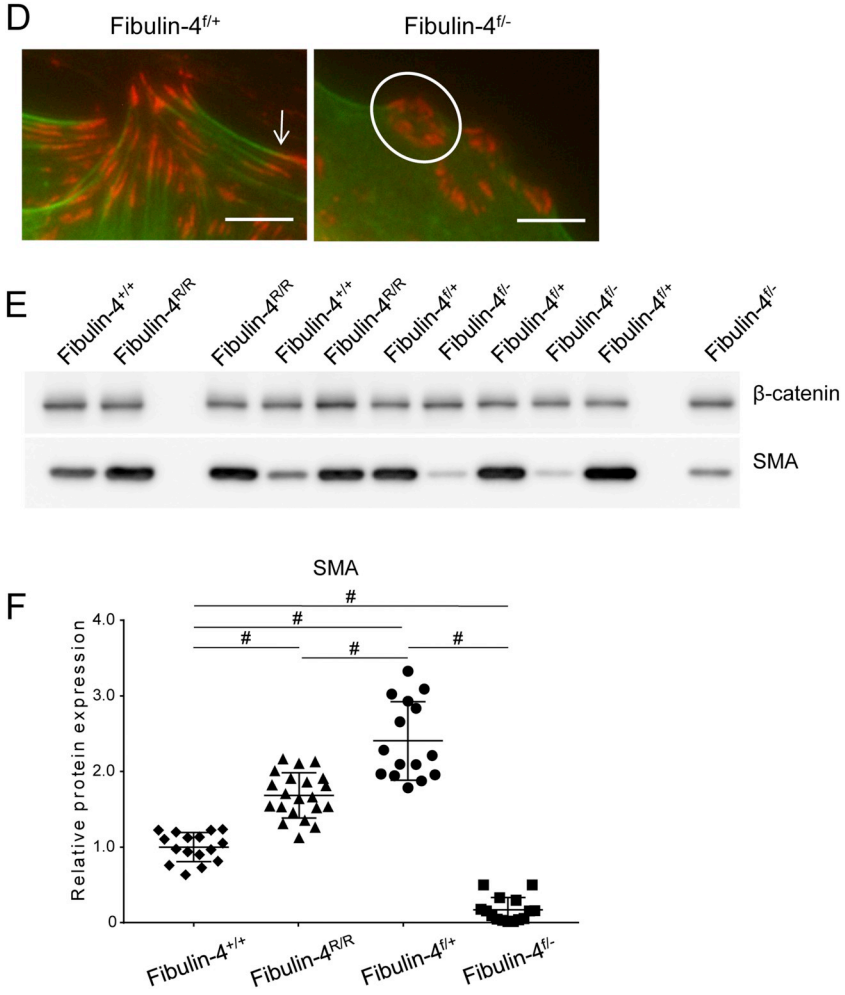

Fig. 1. (*continued*)

protein levels were significantly lower in Fibulin-$4^{f/-}$/SM22Cre^{+} VSMCs compared to Fibulin-$4^{f/+}$/SM22Cre^{+} VSMCs (Fig. 2F and G, $p < .0001$). In Fibulin-$4^{R/R}$ VSMCs, SM22 protein levels were increased compared to Fibulin-$4^{+/+}$ VSMCs (Fig. 2F and G, $p < .05$). Similarly, when comparing Fibulin-$4^{f/+}$/SM22Cre^{+} VSMCs to Fibulin-$4^{+/+}$, SM22 protein levels were increased in Fibulin-$4^{f/+}$/SM22Cre^{+} VSMCs (Fig. 2F and G, $p < .0001$). Hence, reduction of Fibulin-4 leads to increased SM22 levels, whereas complete absence of Fibulin-4 leads to reduced SM22.

These results show that the actin dynamics are altered in both Fibulin-$4^{f/-}$/SM22Cre^{+} VSMCs as well as Fibulin-$4^{R/R}$ VSMCs. While Fibulin-$4^{f/-}$/SM22Cre^{+} VSMCs showed a decreased F-actin fraction, increased depolymerization and decreased SM22 levels, Fibulin-$4^{R/R}$ VSMCs showed no decrease in F-actin fraction and, opposite to Fibulin-$4^{f/-}$/SM22Cre^{+} VSMCs increased SM22 protein levels.

3.3. Migration is disturbed by Fibulin-4 mutations

We subsequently investigated whether the changes in cytoskeletal composition and actin (de)polymerization have implications for spontaneous cellular migration. We stained the overall actin cytoskeleton present in all cells (in contrast to the VSMC specific actin protein, SMA), by addition of the SiR-Actin probe, which is incorporated into the actin cytoskeleton and allows monitoring of cellular migration and measuring migration velocity by live cell imaging.

During cellular migration, new actin fibers and focal adhesions are formed in the direction of migration, while actin fibers are depolymerizing and focal adhesions are detaching at the back of the cell. Live cell imaging of VSMCs labeled with SiR-Actin and overexpression of the focal adhesion protein paxillin-eGFP displays this directional migration (online, Movie_1). Fig. 3A displays a limited set of frames from these live cell movies with the arrows indicating migration direction. A close up of a Fibulin-$4^{f/+}$/SM22Cre^{+} VSMC shows the formation of new focal adhesions in the direction of movement and disappearance of focal adhesions at the detaching side of the cells. Interestingly, Fibulin-$4^{f/-}$/SM22Cre^{+} VSMCs showed formation of new focal adhesions evenly distributed around the entire cell membrane and migration of individual cells occurs in all directions. Since this direction of migration occurred simultaneously in opposite directions, this resulted in reduced effective migrations and expansion of individual cells (Fig. 3A and online, Movie_2).

To obtain an overview of migration and to quantify migration velocity cells were imaged at lower magnification. Fibulin-$4^{f/-}$/SM22Cre^{+} VSMCs showed a shorter path length compared to Fibulin-$4^{f/+}$/SM22Cre^{+} VSMCs and thus less migration. When total migration was corrected for time, migration velocity was obtained. Fibulin-$4^{f/-}$/SM22Cre^{+} VSMCs showed a decreased migration velocity compared to control VSMCs (Fig. 3B, $p < .001$). Fibulin-$4^{R/R}$ VSMCs also showed decreased migration velocity compared to Fibulin-$4^{+/+}$ VSMCs (Fig. 3B, $p < .0001$). Unlike Fibulin-$4^{f/-}$/SM22Cre^{+} VSMCs, directionality of movement was seen in Fibulin-$4^{R/R}$ VSMCs. Migration velocity did not differ between Fibulin-$4^{f/+}$/SM22Cre^{+} and Fibulin-$4^{+/+}$ VSMCs. Example movies can be found online (Movie_3 to Movie_6).

Taken together these data show that when Fibulin-4 is absent or reduced, VSMCs exhibit decreased migration and have a lower

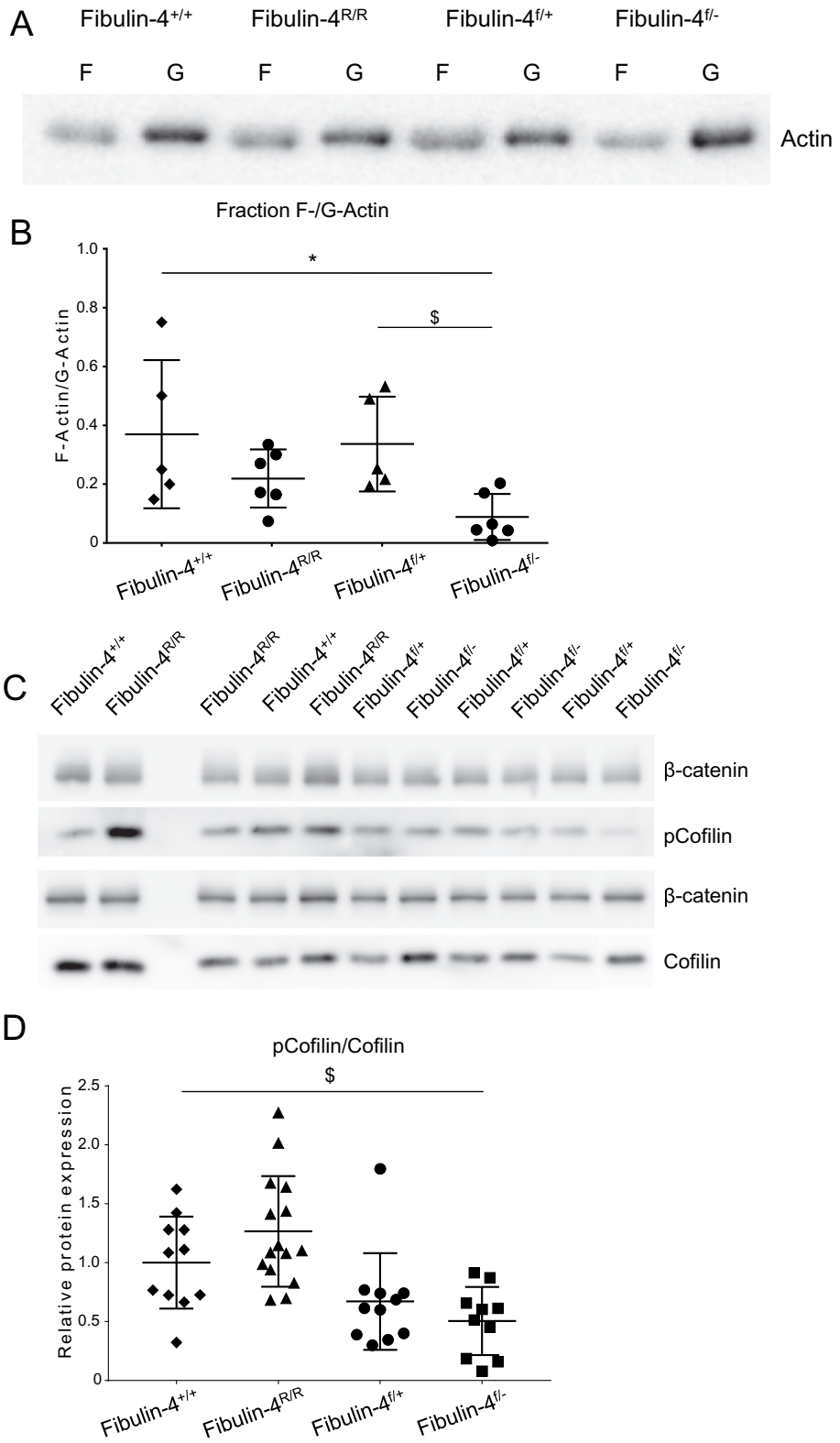

Fig. 2. Altered cytoskeleton dynamics in Fibulin-$4^{R/R}$ and Fibulin-$4^{f/-}$ VSMCs. A) Western blot of F−/G-actin containing fractions in Fibulin-$4^{+/+}$, Fibulin-$4^{f/+}$, Fibulin-$4^{R/R}$, and Fibulin-$4^{f/-}$ VSMC protein extracts. B) Quantification of F-actin to G-actin ratio. Data is shown for $n = 2$ samples in 3 independent experiments. C) Western blot detecting pCofilin, Cofilin and loading control β-catenin in Fibulin-$4^{+/+}$, Fibulin-$4^{R/R}$, Fibulin-$4^{f/+}$ and Fibulin-$4^{f/-}$ VSMC protein extracts. D) Quantification of pCofilin/Cofilin ratio. Data is shown for $n = 4$–6 samples in 3 independent experiments. E) Western blot for SM22 and loading control β-catenin for Fibulin-$4^{+/+}$, Fibulin-$4^{R/R}$, Fibulin-$4^{f/+}$ and Fibulin-$4^{f/-}$ VSMC protein extracts. F) Quantification of SM22 shown in E). Data is shown for n = 4 lysates in 3 independent experiments. Bars represent mean ± SD. Mann-Whitney test. * $p < .05$, $ $p < .01$, # $p < .0001$.

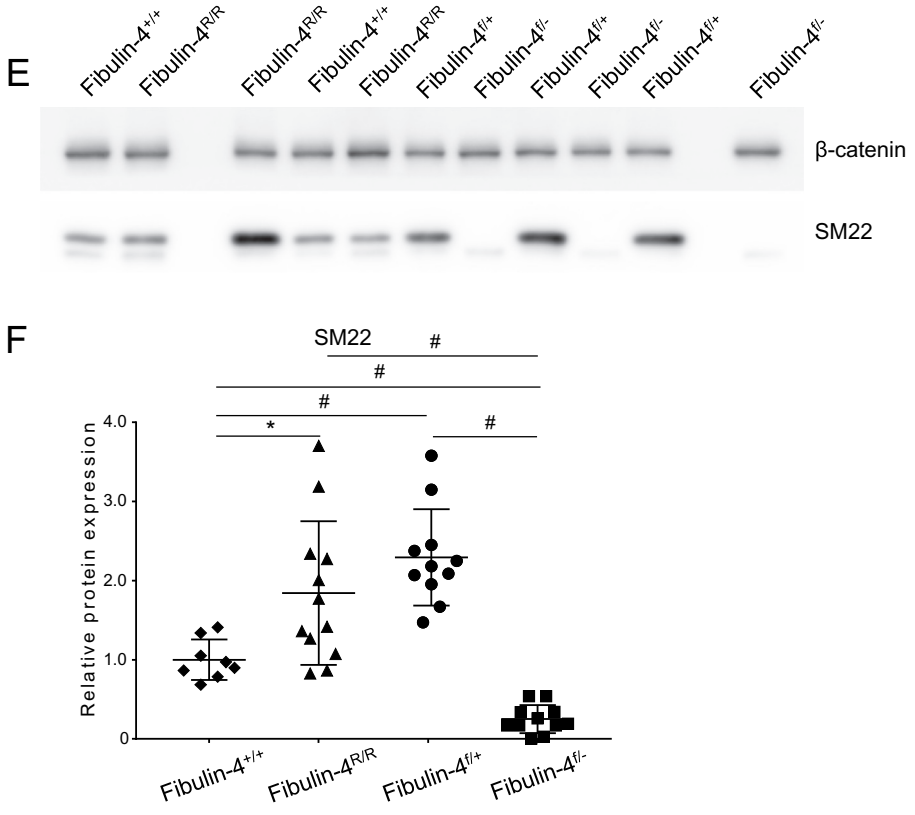

Fig. 2. (*continued*)

migration velocity compared to control cells.

3.4. Analysis of ECM production and TGFβ signaling pathway in Fibulin-4$^{f/-}$/SM22Cre^{+} and Fibulin-4$^{R/R}$ VSMCs

Since fibulin-4 plays an important role in ECM integrity and both Fibulin-4$^{R/R}$ and Fibulin-4$^{f/-}$/SM22Cre^{+} mutant VSMCs show decreased migration, we investigated whether this similarity in aberrant movement was caused by similar changes in ECM composition. Immunofluorescent staining of the ECM components, fibulin-4, fibronectin-1, fibrillin-1 and latent TGFβ binding protein 4 (LBTP4), was performed after 7 days of culture to asses ECM production in both types of Fibulin-4 mutant VSMCs.

Fibulin-4 is essential for elastogenesis and recruitment of lysyl oxidase. Lysyl oxidase is needed for crosslinking of the elastin precursor tropoelastin and the formation of mature elastic laminae. In contrast to Fibulin-4$^{+/+}$ VSMCs, Fibulin-4$^{R/R}$ VSMCs do not show a clear network of fibulin-4 fibers (Fig. 4A). Fibulin-4$^{f/+}$/SM22Cre^{+} VSMCs do show fibulin-4 fibers, however, with less intensity than Fibulin-4$^{+/+}$ VSMCs (Fig. 4A). In Fibulin-4$^{f/-}$/SM22Cre^{+} VSMCs fibulin-4 fibers and protein are not detectable (Fig. 4A). Fibronectin serves as a base network on which other ECM proteins are deposited. Therefore, production of fibronectin is essential for proper ECM formation. A more extensive network of fibronectin fibers were apparent in Fibulin-4$^{R/R}$ VSMCs compared to Fibulin-4$^{+/+}$ VSMCs, (Fig. 4B). In contrast, Fibulin-4$^{f/-}$/SM22Cre^{+} VSMCs produced a minimal amount of fibronectin fibers compared to Fibulin-4$^{f/+}$/SM22Cre^{+} and Fibulin-4$^{+/+}$ VSMCs. Fibulin-4$^{f/+}$/SM22Cre^{+} VSMCs show a slight increase in fibronectin fibers compared to Fibulin-4$^{+/+}$ VSMCs. Fibrillin-1 is the central component of microfibrils and is important for structural support in tissues and elastic fiber formation. Similarly to the fibronectin network, the fibrillin-1 fiber network of Fibulin-4$^{R/R}$ VSMCs is more extensive than of Fibulin-4$^{+/+}$ VSMCs (Fig. 4C). However, Fibulin-4$^{f/-}$/SM22Cre^{+} VSMCs show a less extensive fibrillin-1 fiber network compared to Fibulin-4$^{f/+}$/SM22Cre^{+} and Fibulin-4$^{+/+}$ VSMCs. Like the fibronectin fibers, Fibulin-4$^{f/+}$/SM22Cre^{+} VSMCs show a slight increase in fibrillin-1 fibers compared to Fibulin-4$^{+/+}$ VSMCs (Fig. 4C). LTBP4 binds inactive TGFβ to the ECM where it is stored until activation occurs. LTBP4 is of importance for the bioavailability of TGFβ and, therefore, activation of the TGFβ signaling pathway. While LTBP4 is detected in Fibulin-4$^{f/-}$/SM22Cre^{+} VSMCs and fibers are formed, the number of LTBP4 fibers is far less compared to Fibulin-4$^{f/+}$/SM22Cre^{+} VSMCs. Fibulin-4$^{R/R}$ VSMCs showed increased staining of LTBP4 present in an extensive ECM network compared to Fibulin-4$^{+/+}$ VSMCs. Again, Fibulin-4$^{f/+}$/SM22Cre^{+} VSMCs show a slight increase in LTBP4 compared to Fibulin-4$^{+/+}$ VSMCs (Fig. 4D). The slight increase in ECM production by Fibulin-4$^{f/+}$/SM22Cre^{+} VSMCs could explained by the reduced expression of fibulin-4. In conclusion, this suggests that a reduction in fibulin-4 results in upregulation of ECM deposition but a complete absence of fibulin-4 abolishes the deposition/assembly of various ECM proteins.

The difference in ECM deposition found between Fibulin-4$^{R/R}$ and Fibulin-4$^{f/-}$/SM22Cre^{+} VSMCs could indicate differential activities of the TGFβ pathway signaling in both mutants. Hence, we next performed analysis of TGFβ signaling components as well as TGFβ pathway activation. To determine if Fibulin-4$^{f/-}$/SM22Cre^{+} VSMCs show increased TGFβ signaling, we performed western blotting to determine the phosphorylation status of SMAD2 (pSMAD2) (Fig. 4E and F). While SMAD2 protein levels were comparable, Fibulin-4$^{f/-}$/SM22Cre^{+} cell lysates showed lower pSMAD2 protein levels compared to Fibulin-4$^{f/+}$/SM22Cre^{+} lysates. (Fig. 4E). Fibulin-4$^{R/R}$ VSMC whole cell lysates showed higher pSMAD2 protein levels compared to Fibulin-4$^{+/+}$ lysates as also previously observed (Fig. 4E) [23]. Quantification of the pSMAD2 and SMAD2 levels showed a significant decrease in pSMAD2/SMAD2 ratio in Fibulin-4$^{f/-}$/SM22Cre^{+} VSMCs compared to Fibulin-4$^{f/+}$/SM22Cre^{+} lysates (Fig. 4F, $p < .05$), while Fibulin-4$^{R/R}$ VSMCs showed an increased pSMAD2/SMAD2 ratio compared to its control (Fig. 4F, $p < .05$).

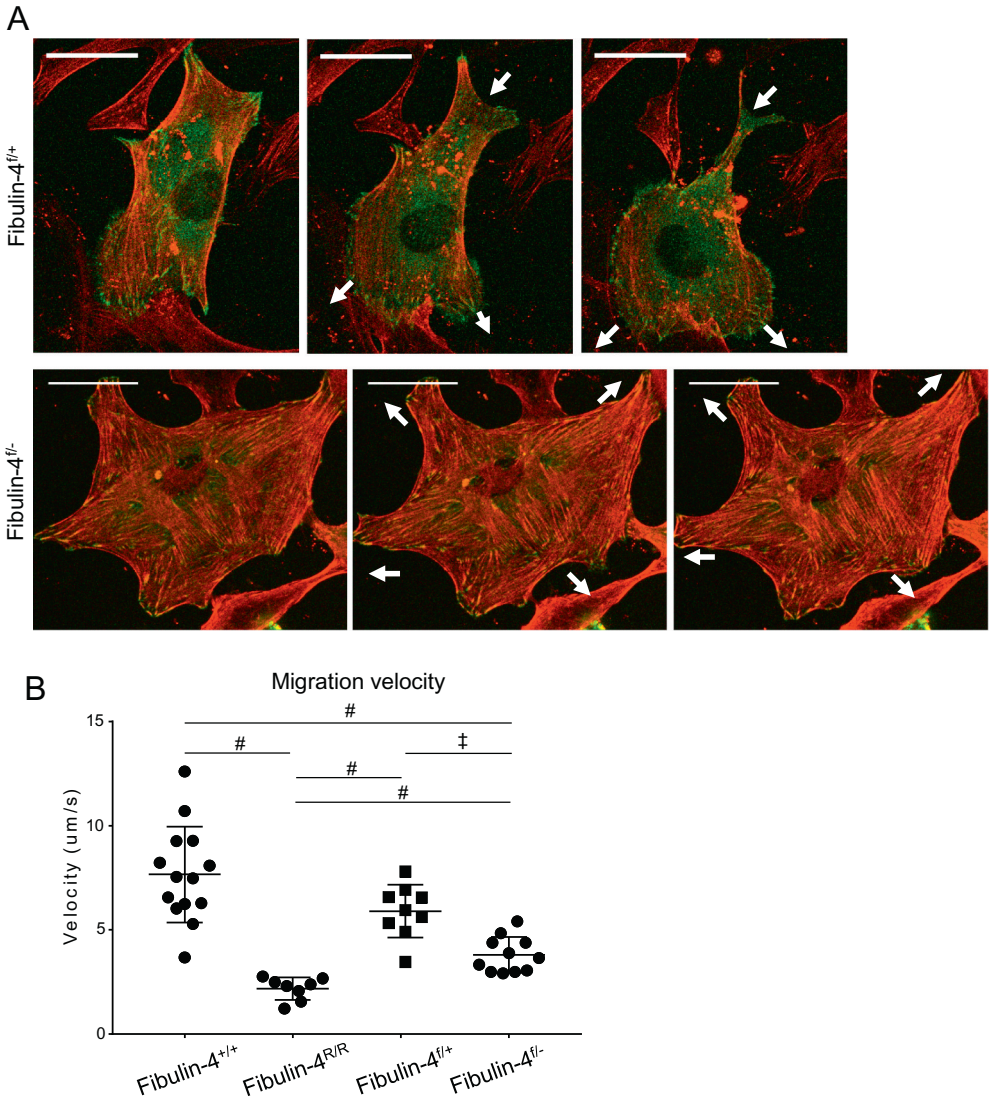

Fig. 3. Fibulin-$4^{f/-}$ and Fibulin-$4^{R/R}$ VSMCs show less migration. A) Selected frames of live cell imaging (online movie_1 and movie_2) showing the migration of Fibulin-$4^{f/+}$ and Fibulin-$4^{f/-}$ VSMCs. Paxillin overexpression is depicted in green and actin (SiR-Actin) is depicted in red. Direction of movement is indicated by the arrows. Scale bars equals 50 μm. B) Quantification of migration velocity of Fibulin-$4^{+/+}$, Fibulin-$4^{R/R}$, Fibulin-$4^{f/+}$ and Fibulin-$4^{f/-}$ VSMCs (online movie_3, movie_4, movie_5 and movie_6). Bars represent mean ± SD. Mann-Whitney test, ‡ $p < .01$ # $p < .0001$.

To examine downstream activation of the TGFβ pathway, a TGFβ reporter assay was performed. In this assay PAI-1 promoter activation, represented by luciferase activity, is measured. PAI-1 can be activated by binding of the phosphorylated SMAD2/SMAD3 complex. Fibulin-$4^{R/R}$ VSMCs showed spontaneous increased TGFβ signaling pathway activation compared to Fibulin-$4^{+/+}$ VSMCs (Fig. 4G, $p < .001$). Our previous research on Fibulin-$4^{R/R}$ VSMCs showed that increased TGFβ signaling could be reduced by treatment of the cells with SB431542 hydrate, a TGFβ receptor blocker [23]. As visualized in Fig. 4H, the intrinsic, cell autonomous TGFβ signaling pathway activation in Fibulin-$4^{f/-}$/SM22Cre^{+} VSMCs was decreased compared to Fibulin-$4^{f/+}$/SM22Cre^{+} VSMCs ($p < .05$). When TGFβ signaling was inhibited by SB431542 hydrate in Fibulin-$4^{f/-}$/SM22Cre^{+} VSMCs there was no significant decrease in PAI-1 promoter, while Fibulin-$4^{R/R}$ VSMCs did show such a decrease in PAI-1 promoter activation after treatment with SB431542 hydrate (Fig. 4 I and J).

When stimulated with TGFβ, the TGFβ pathway can be activated in Fibulin-$4^{f/-}$/SM22Cre^{+} VSMCs as well as in Fibulin-$4^{R/R}$ VSMCs (Fig. 4K and L, $p < .0001$). Western blot analysis of protein lysates of VSMCs stimulated with and without TGFβ further showed increased pSMAD2 levels after TGFβ stimulation. Interestingly, stimulation with TGFβ increased SMA protein levels in Fibulin-$4^{f/-}$/SM22Cre^{+} VSMCs compared to non-stimulated Fibulin-$4^{f/-}$/SM22Cre^{+} VSMCs. However, it did not increase SM22 protein levels. Fibulin-$4^{R/R}$ VSMCs also showed increased pSMAD2 protein levels upon TGFβ stimulation. A further increase of TGFβ signaling in Fibulin-$4^{R/R}$ VSMCs did not result in a large increase in SMA and SM22 protein levels.

4. Discussion

Our current data reveal that actin cytoskeleton structure and dynamics are affected in both Fibulin-$4^{f/-}$/SM22Cre^{+} as well as Fibulin-$4^{R/R}$ VSMCs. Strikingly, we show that while TGFβ activation is increased in VSMCs when Fibulin-4 levels are reduced (Fibulin-$4^{R/R}$), no changes in the activation of TGFβ signaling are observed in the absence of Fibulin-4 (Fibulin-$4^{f/-}$/SM22Cre^{+}). Thus, a complete absence versus reduced levels of Fibulin-4 differentially affects TGFβ signaling, intracellular cytoskeleton structures and consequently cell movement.

Both the Fibulin-$4^{R/R}$ and Fibulin-$4^{f/-}$/SM22Cre^{+} mouse model show aortic aneurysm formation. Histological analysis of the aortas

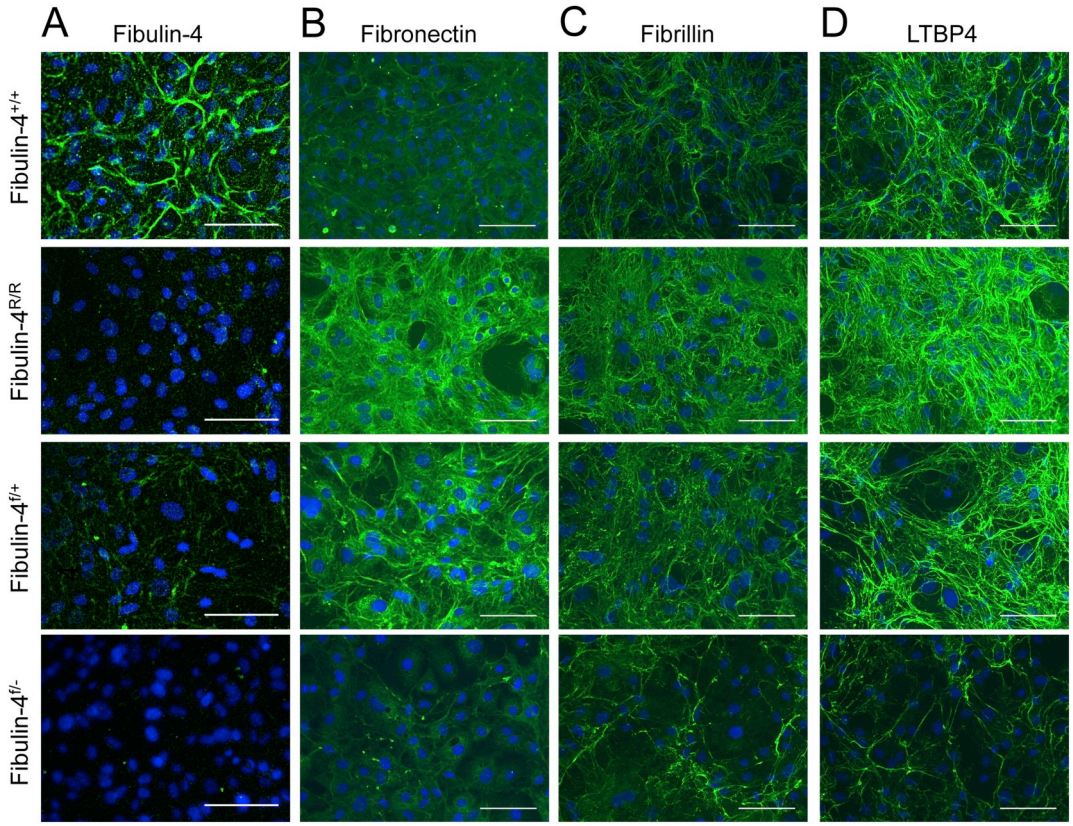

Fig. 4. Analysis of ECM production and TGFβ signaling in Fibulin-$4^{R/R}$ and Fibulin-$4^{f/-}$ VSMCs. Immunofluorescent staining of production of ECM proteins by VSMCs after 7 days in culture. Representative images are shown, scale bar is 100 μm. A) Immunofluorescent staining of fibulin-4. B) Immunofluorescent staining of fibronectin. C) Immunofluorescent staining of fibrillin-1. D) Immunofluorescent staining of latent TGFβ binding protein (LTBP4). E) Western blots for pSMAD2, SMAD2 and loading control β-catenin for Fibulin-$4^{+/+}$, Fibulin-$4^{f/+}$, Fibulin-$4^{R/R}$ and Fibulin-$4^{f/-}$ VSMC protein extracts. F) Quantification of pSMAD2/SMAD2 ratio. Data is shown for n = 2–3 lysates in 3 independent experiments. G) Luciferase TGFβ transcriptional based assay showing increased activation of the PAI-1 promoter in Fibulin-$4^{R/R}$ VSMCs compared to Fibulin-$4^{+/+}$ VSMCs. n = 3 independent experiments in triplicate. H) Luciferase TGFβ transcriptional based assay showing a decrease in pathway activation in Fibulin-$4^{f/-}$ VSMCs compared to Fibulin-$4^{f/+}$ VSMCs. n = 3 independent experiments in triplicate. I) and J) Luciferase TGFβ transcriptional based assay showing no decrease in pathway activation after TGFβ inhibition in Fibulin-$4^{f/-}$, while Fibulin-$4^{R/R}$ VSMCs do show decreased TGFβ pathway after inhibition. Data is shown for 3 independent experiments with n = 3–4 samples. K) Luciferase TGFβ transcriptional based assay showing increased pathway activation after TGFβ stimulation in Fibulin-$4^{R/R}$ VSMCs. Data is shown for 3 independent experiments with n = 4 samples. Western blots for pSMAD2, SMAD2, SMA, SM22 and loading control β-catenin for Fibulin-$4^{R/R}$ VSMC protein extracts, with and without TGFβ stimulation. L) Luciferase TGFβ transcriptional based assay showing increased pathway activation after TGFβ stimulation in Fibulin-$4^{f/-}$ VSMCs. Data is shown for 3 independent experiments with n = 4–5 samples. Western blots for pSMAD2, SMAD2, SMA, SM22 and loading control β-catenin for Fibulin-$4^{f/-}$ VSMC protein extracts, with and without TGFβ stimulation. Bars represent mean ± SD. Mann-Whitney test. * $p < .05$, $ $p < .01$ ‡ $p < .001$, # $p < .0001$.

shows fragmentation of the elastic laminae and thickening of the aortic wall in both models. However, there are striking differences between these models. The fragmentation of the elastic laminae differs between the two models. Although Fibulin-$4^{f/-}$/SM22Cre^{+} aortas show severe fragmentation, it appears that the first elastic laminae adjacent to the endothelial layer remain intact [22,24]. In Fibulin-$4^{R/R}$ aortas elastic laminae throughout the entire media are fragmented. In this respect, the affected cell populations in each model might explain this difference; in Fibulin-$4^{R/R}$ mice all cells have reduced Fibulin-4 expression, while in Fibulin-$4^{f/-}$/SM22Cre^{+} mice Fibulin-4 is specifically deleted in VSMCs, surrounded by wild-type endothelial cells and fibroblasts. Which is the reason why in this study we compared VSMCs from both models.

Our data showed that both Fibulin-4 models display changes in their cytoskeleton composition. Previous research by Huang et al. has shown that aortas of *Fibulin-4* germline knock-out embryos (Fibulin-4^{GKO}) contain less SMA [24]. Fibulin-4^{GKO} VSMCs also displayed less distinct actin fibers upon detection with phalloidin. Gene expression of *ACTA2* and *SM22* is decreased in Fibulin-$4^{f/-}$/SM22Cre^{+} aortas [24,31], which is in accordance with our results of decreased SMA and SM22 protein levels in Fibulin-$4^{f/-}$/SM22Cre^{+} VSMCs. Although we find decreased SM22 protein levels in Fibulin-$4^{f/-}$/SM22Cre^{+} VSMCs, the SM22 promoter must have been active during development, as the Cre expression in the VSMC specific Fibulin-4 knock out is regulated by the *SM22* promotor. Decreased presence of SMA has previously also been found by Arnold et al. in a neural crest cell specific knock-out of integrin linked kinase (ILK) [34]. Wnt1cre; $Ilk^{flox/flox}$ embryos present with a severe aneurysmal arterial trunk, which leads to embryonic lethality during late gestation. Decreased differentiation of smooth muscle tissue has been observed as well as disorganization of F-actin stress fibers. In addition, these embryos have decreased pSmad3 staining. The similarities in the Fibulin-$4^{f/-}$/SM22Cre^{+} model and the Wnt1cre; $Ilk^{flox/flox}$ model highlights a fundamental basis for the mechanistic link between the TGFβ signaling and proper cytoskeleton formation in aneurysmal disease. In contrast to Fibulin-$4^{f/-}$/SM22Cre^{+} VSMCs, Fibulin-$4^{R/R}$ VSMCs show increased SMA protein levels. Research by Ramnath et al. has shown increased *SMA* mRNA in Fibulin-$4^{R/R}$ VSMCs [23]. Our current data now indicate that this increased SMA expression is also translated into increased protein levels. From literature it is known that TGFβ signaling is involved in VSMC differentiation and induces expression of SMA and SM22 [35,36]. The increased TGFβ signaling in Fibulin-$4^{R/R}$ VSMCs and aortas could

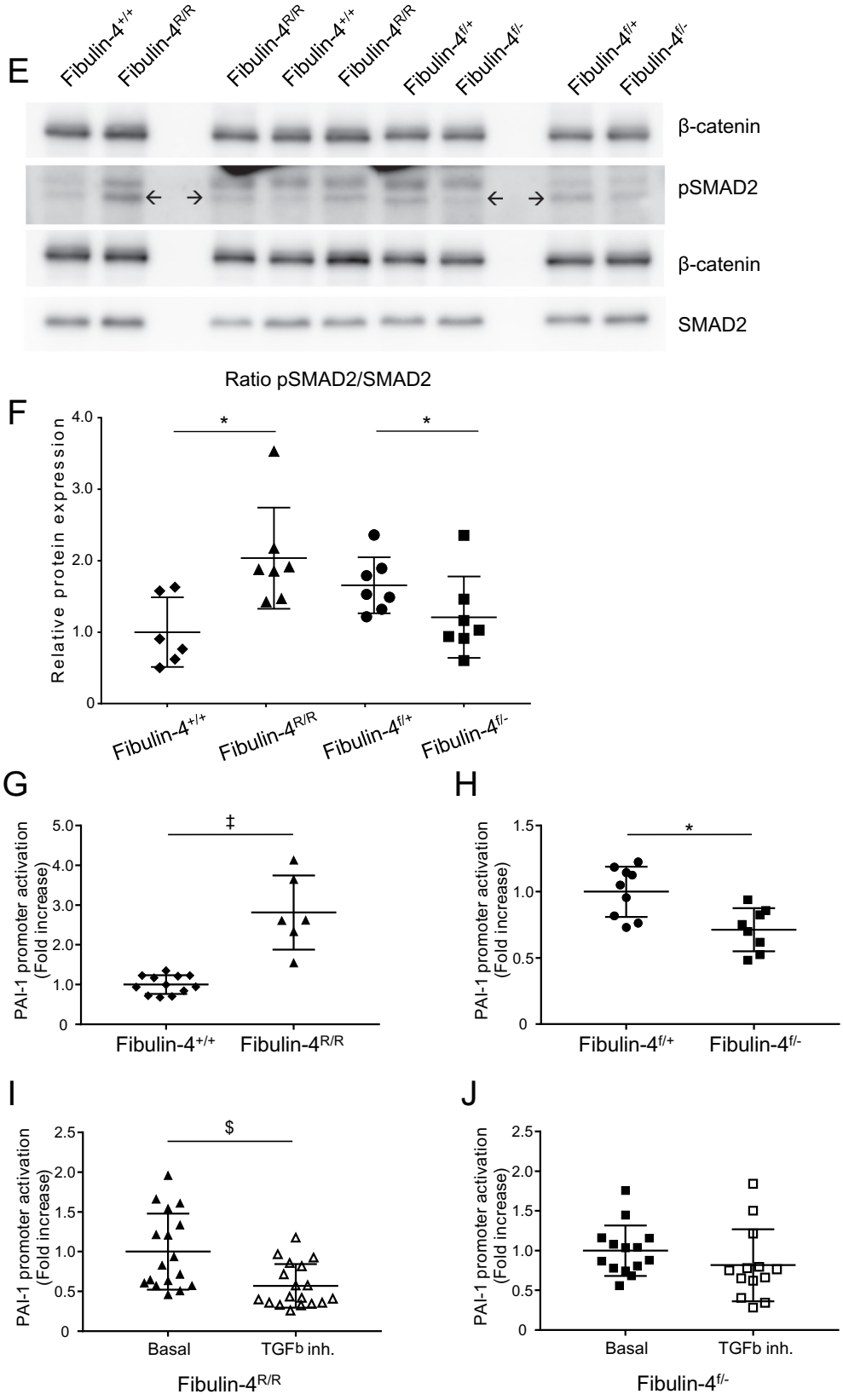

Fig. 4. (*continued*)

therefore be responsible for the increased expression of SMA and SM22.

As previously mentioned, less distinct actin fibers have been found in Fibulin-4^{GKO} VSMCs by Huang et al. [24]. Yamashiro et al. investigated the actin fibers further in Fibulin-$4^{f/-}$/SM22Cre^{+} aortas and have shown that the ratio of F-actin to G-actin is significantly decreased in the ascending aorta of Fibulin-$4^{f/-}$/SM22Cre^{+} mice compared to their controls [31]. This decrease in F-actin to G-actin is in line with our results in VSMCs derived from Fibulin-$4^{f/-}$/SM22Cre^{+} aortas,

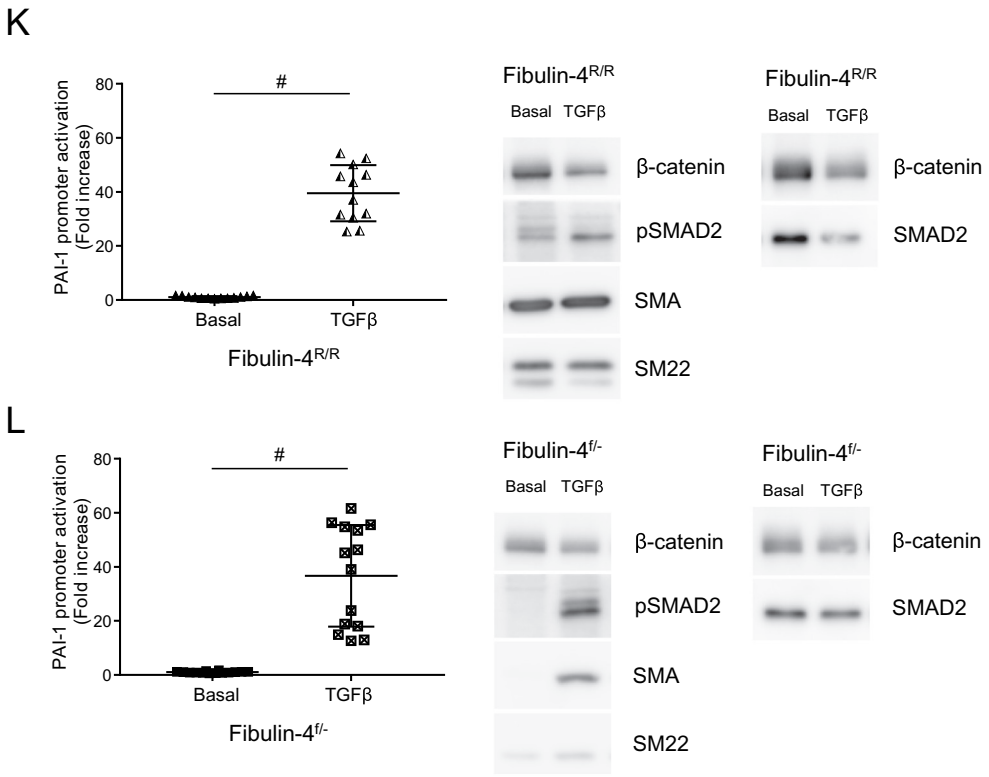

Fig. 4. (*continued*)

however, there is no significant decrease detected in Fibulin-4$^{R/R}$ VSMCs. The decreased phosphorylated cofilin to cofilin ratio we observe in the Fibulin-4$^{f/-}$/SM22Cre^{+} VSMCs, which could result in increased depolymerization of actin, can explain the decrease in F-actin. The interaction between actin dynamics and ECM composition, as we find for Fibulin-4$^{f/-}$/SM22Cre^{+} and Fibulin-4$^{R/R}$ VSMCs, has also been observed for different biological systems and in different experimental set-ups [37–39].

Increased activation of the TGFβ signaling pathway is often thought to be causative in aneurysm formation. Yet, our results do not show increased activation of the TGFβ pathway in Fibulin-4$^{f/-}$/SM22Cre^{+} VSMCs. Recent data suggests a dual role for TGFβ signaling in aneurysm formation; while increased signaling can be protective in early stages of the disease, it can be detrimental in later disease stages [40,41]. This implies that disturbed TGFβ signaling is not the single culprit in aneurysm formation. Our data also underlines the importance of the cytoskeleton in aneurysm formation, since we show that Fibulin-4 defects lead to cytoskeleton alterations. While Fibulin-4$^{R/R}$ VSMCs show overproduction of the ECM, increased TGFβ signaling and increased production of SMA, Fibulin-4$^{f/-}$/SM22Cre^{+} VSMCs show less ECM production, no increased TGFβ signaling and a lack of SMA production and SMA fiber formation. This suggests that a defect in the ECM protein fibulin-4 can lead to alterations of the cytoskeleton. Recent research has shown the importance of the VSMC cytoskeleton in combination with the ECM to contractility of the VSMCs and aneurysm formation. Without proper connections of the cytoskeleton to the ECM, a VSMC cannot generate force for its contractions. This shows that the ECM and the cytoskeleton are of great importance for the contractility of the aorta and may be primary drivers of thoracic aortic aneurysms when these are defective [42].

Our data show that activation of the TGFβ pathway by TGFβ stimulation is possible in Fibulin-4$^{f/-}$/SM22Cre^{+} VSMCs and thus receptor expression and signal transduction is still intact. We show that addition of exogenous TGFβ to Fibulin-4$^{f/-}$/SM22Cre^{+} VSMCs results in increased SMA protein levels. This result shows the direct interconnection between TGFβ pathway signaling and SMA protein levels. From literature it is known that TGFβ is involved in VSMC differentiation [43–45]. This differentiation is directly induced by TGFβ via binding of SMAD3 to the *SM22* promoter and induction of SMA production via RhoA [46,47].

The difference in TGFβ pathway activation between the Fibulin-4$^{f/-}$/SM22Cre^{+} and Fibulin-4$^{R/R}$ mouse model could be the result of the difference in ECM composition. The increased TGFβ levels in the Fibulin-4$^{R/R}$ models is thought to be due to less stable binding of the large latent complex (LLC) to fibrillin-1 [23]. Our data show increased ECM deposition by Fibulin-4$^{R/R}$ VSMCs and increased amounts of LTBP4, implicating higher bioavailability of TGFβ, together explaining the augmented TGFβ activation. Furthermore, Bultmann-Mellin et al. showed that LTBP4-L is needed for the deposition of fibulin-4 in the ECM and thereby proper elastogenesis, and they showed a physical interaction between LTBP4 and Fibulin-4 [48,49]. Increased TGFβ activation in the Fibulin-4$^{R/R}$ model has previously been discovered by RNA expression analysis of Fibulin-4$^{R/R}$ aortas and TGFβ cytokine analysis in aortic extracts and blood of Fibulin-4$^{R/R}$ mice [23,50]. In contrast, the less extensive ECM deposition we find in Fibulin-4$^{f/-}$/SM22Cre^{+} VSMCs could lead to decreased TGFβ signaling activity since there is no properly formed ECM to bind the latent TGFβ. Massam-Wu et al. have shown that fibulin-4 binds with high affinity to LTBP1, a key mediator in binding of latent TGFβ in the ECM by binding to LTBP4 as well as fibrillin-1 [51]. This suggests that Fibulin-4$^{f/-}$/SM22Cre^{+} VSMCs are unable to confine latent TGFβ in their matrix due to the absence of Fibulin-4. Reduced storage of TGFβ could, in part, explain the decreased TGFβ signaling seen in Fibulin-4$^{f/-}$/SM22Cre^{+} VSMCs. Especially since we show that exogenous addition of TGFβ is able to activate the TGFβ pathway. Further research would be needed to determine if the decrease in TGFβ signaling in Fibulin-4$^{f/-}$/SM22Cre^{+} VSMCs is caused by reduced production or secretion of TGFβ.

Since depolymerization of actin fibers is needed for retraction of the cells during migration [52,53], increased deposition of ECM proteins by

Fibulin-4$^{R/R}$ VSMCs in combination with increased production of SMA and decreased depolymerization of the cytoskeleton could explain why Fibulin-4$^{R/R}$ VSMCs show less migration compared to control VSMCs. Furthermore, the more elaborate ECM of Fibulin-4$^{R/R}$ VSMCs could lead to a stronger attachment to the culture plate, leading to less effective migration. The increased SMA protein levels also implicates a more contractile phenotype in Fibulin-4$^{R/R}$ VSMCs, as literature suggests less migration for this contractile VSMC phenotype compared to the synthetic VSMC phenotype [54]. Although Fibulin-4$^{f/-}$/SM22Cre^{+} VSMCs show less deposition of ECM proteins, their migration is still less effective compared to Fibulin-4$^{f/+}$/SM22Cre^{+} VSMCs. In this case, the reduced effective movement could be caused by the absence of SMA fibers, less differentiation of the VSMCs and decreased attachment due to the low ECM content. However, it remains to be determined if the absence of Fibulin-4 and lack of ECM production by Fibulin-4$^{f/-}$/SM22Cre^{+} VSMCs is causative for the cytoskeleton alterations.

Our results show that while these reduction or absence of Fibulin-4 show opposite effects in cytoskeleton dynamics and TGFβ signaling, both result in aneurysm formation in the mouse. Our data underlines the need for new possible treatments of aneurysmal disease. Currently most therapies are based on increased TGFβ signaling, while we show that the Fibulin-4$^{f/-}$/SM22Cre^{+} lack increased TGFβ signaling. Yet, Fibulin-4$^{f/-}$/SM22Cre^{+} mice do show aneurysm formation. Since both Fibulin-4$^{R/R}$ and Fibulin-4$^{f/-}$/SM22Cre^{+} mouse models show alterations in the cytoskeleton, we propose that this is an additional underlying cause of aneurysm formation, which would be a potential target for the development of novel therapies.

5. Conclusion

From these results we conclude that Fibulin-4 mutations lead to SMA cytoskeleton instabilities as well as dysregulation of the TGFβ pathway. However, reduced levels of Fibulin-4 have a strikingly different effect compared to the complete absence of Fibulin-4. When Fibulin-4 is absent the production of ECM is reduced, the TGFβ pathway is not activated and SMA is not produced. In contrast, reduced levels of Fibulin-4 lead to excessive ECM deposition, over-activation of the TGFβ pathway and cytoskeleton fibers aberrations. Although these models show opposite effects, both mutations lead to aneurysm formation. Moreover, we conclude that not only TGFβ signaling, but also cytoskeleton dynamics could be causative for aortic aneurysmal disease.

Supplementary data to this article can be found online at https://doi.org/10.1016/j.cellsig.2019.02.008.

Declaration of interest

None.

Acknowledgements

We would like to thank Dr. ir. Jacob Hoogenboom from the department of Imaging Physics at Delft University of Technology for helping us with the microscopy for the close-ups of the focal adhesions, Dr. Yoshito Yamashiro from the Life Science Center for Survival Dynamics, Tsukuba Advanced Research Alliance (TARA) from the University of Tsukuba for sending the Fibulin-4$^{f/-}$/SM22Cre^{+} VSMCs, Lleroy Weerwind for performing initial western blotting analysis of cytoskeleton proteins in the Fibulin-4$^{f/-}$/SM22Cre^{+} and Fibulin-4$^{R/R}$ VSMCs, Karin Legerstee for providing us with the paxillin-eGFP plasmid.

This work was supported by the 'Lijf and Leven' grant (2014) "GAMMA" (Genexpressie analyse ter detectie van de moleculaire mechanismen van aneurysmavorming).

References

[1] M.E. Lindsay, H.C. Dietz, Lessons on the pathogenesis of aneurysm from heritable conditions, Nature 473 (7347) (2011) 308–316.
[2] E.M. Isselbacher, Thoracic and abdominal aortic aneurysms, Circulation 111 (6) (2005) 816–828.
[3] H.C. Dietz, R.E. Pyeritz, B.D. Hall, R.G. Cadle, A. Hamosh, J. Schwartz, D.A. Meyers, C.A. Francomano, The Marfan syndrome locus: confirmation of assignment to chromosome 15 and identification of tightly linked markers at 15q15-q21.3, Genomics 9 (2) (1991) 355–361.
[4] B.L. Loeys, J. Chen, E.R. Neptune, D.P. Judge, M. Podowski, T. Holm, J. Meyers, C.C. Leitch, N. Katsanis, N. Sharifi, F.L. Xu, L.A. Myers, P.J. Spevak, D.E. Cameron, J. De Backer, J. Hellemans, Y. Chen, E.C. Davis, C.L. Webb, W. Kress, P. Coucke, D.B. Rifkin, A.M. De Paepe, H.C. Dietz, A syndrome of altered cardiovascular, craniofacial, neurocognitive and skeletal development caused by mutations in TGFBR1 or TGFBR2, Nat. Genet. 37 (3) (2005) 275–281.
[5] B.L. Loeys, U. Schwarze, T. Holm, B.L. Callewaert, G.H. Thomas, H. Pannu, J.F. De Backer, G.L. Oswald, S. Symoens, S. Manouvrier, A.E. Roberts, F. Faravelli, M.A. Greco, R.E. Pyeritz, D.M. Milewicz, P.J. Coucke, D.E. Cameron, A.C. Braverman, P.H. Byers, A.M. De Paepe, H.C. Dietz, Aneurysm syndromes caused by mutations in the TGF-beta receptor, N. Engl. J. Med. 355 (8) (2006) 788–798.
[6] T. Mizuguchi, G. Collod-Beroud, T. Akiyama, M. Abifadel, N. Harada, T. Morisaki, D. Allard, M. Varret, M. Claustres, H. Morisaki, M. Ihara, A. Kinoshita, K. Yoshiura, C. Junien, T. Kajii, G. Jondeau, T. Ohta, T. Kishino, Y. Furukawa, Y. Nakamura, N. Niikawa, C. Boileau, N. Matsumoto, Heterozygous TGFBR2 mutations in Marfan syndrome, Nat. Genet. 36 (8) (2004) 855–860.
[7] I.M. van de Laar, R.A. Oldenburg, G. Pals, J.W. Roos-Hesselink, B.M. de Graaf, J.M. Verhagen, Y.M. Hoedemaekers, R. Willemsen, L.A. Severijnen, H. Venselaar, G. Vriend, P.M. Pattynama, M. Collee, D. Majoor-Krakauer, D. Poldermans, I.M. Frohn-Mulder, D. Micha, J. Timmermans, Y. Hilhorst-Hofstee, S.M. Bierma-Zeinstra, P.J. Willems, J.M. Kros, E.H. Oei, B.A. Oostra, M.W. Wessels, A.M. Bertoli-Avella, Mutations in SMAD3 cause a syndromic form of aortic aneurysms and dissections with early-onset osteoarthritis, Nat. Genet. 43 (2) (2011) 121–126.
[8] E.S. Regalado, D.C. Guo, C. Villamizar, N. Avidan, D. Gilchrist, B. McGillivray, L. Clarke, F. Bernier, R.L. Santos-Cortez, S.M. Leal, A.M. Bertoli-Avella, J. Shendure, M.J. Rieder, D.A. Nickerson, N.G.E.S. Project, D.M. Milewicz, Exome sequencing identifies SMAD3 mutations as a cause of familial thoracic aortic aneurysm and dissection with intracranial and other arterial aneurysms, Circ. Res. 109 (6) (2011) 680–686.
[9] D.C. Guo, H. Pannu, V. Tran-Fadulu, C.L. Papke, R.K. Yu, N. Avidan, S. Bourgeois, A.L. Estrera, H.J. Safi, E. Sparks, D. Amor, L. Ades, V. McConnell, C.E. Willoughby, D. Abuelo, M. Willing, R.A. Lewis, D.H. Kim, S. Scherer, P.P. Tung, C. Ahn, L.M. Buja, C.S. Raman, S.S. Shete, D.M. Milewicz, Mutations in smooth muscle alpha-actin (ACTA2) lead to thoracic aortic aneurysms and dissections, Nat. Genet. 39 (12) (2007) 1488–1493.
[10] D.M. Milewicz, J.R. Ostergaard, L.M. Ala-Kokko, N. Khan, D.K. Grange, R. Mendoza-Londono, T.J. Bradley, A.H. Olney, L. Ades, J.F. Maher, D. Guo, L.M. Buja, D. Kim, J.C. Hyland, E.S. Regalado, De novo ACTA2 mutation causes a novel syndrome of multisystemic smooth muscle dysfunction, Am. J. Med. Genet. A 152A (10) (2010) 2437–2443.
[11] L. Zhu, R. Vranckx, P. Khau Van Kien, A. Lalande, N. Boisset, F. Mathieu, M. Wegman, L. Glancy, J.M. Gasc, F. Brunotte, P. Bruneval, J.E. Wolf, J.B. Michel, X. Jeunemaitre, Mutations in myosin heavy chain 11 cause a syndrome associating thoracic aortic aneurysm/aortic dissection and patent ductus arteriosus, Nat. Genet. 38 (3) (2006) 343–349.
[12] H. Pannu, V. Tran-Fadulu, C.L. Papke, S. Scherer, Y. Liu, C. Presley, D. Guo, A.L. Estrera, H.J. Safi, A.R. Brasier, G.W. Vick, A.J. Marian, C.S. Raman, L.M. Buja, D.M. Milewicz, MYH11 mutations result in a distinct vascular pathology driven by insulin-like growth factor 1 and angiotensin II, Hum. Mol. Genet. 16 (20) (2007) 2453–2462.
[13] C.L. Papke, H. Yanagisawa, Fibulin-4 and fibulin-5 in elastogenesis and beyond: insights from mouse and human studies, Matrix Biol. 37 (2014) 142–149.
[14] S.M. Mithieux, A.S. Weiss, Elastin, Adv. Protein Chem. 70 (2005) 437–461.
[15] I.B. Robertson, M. Horiguchi, L. Zilberberg, B. Dabovic, K. Hadjiolova, D.B. Rifkin, Latent TGF-beta-binding proteins, Matrix Biol. 47 (2015) 44–53.
[16] M. Horiguchi, T. Inoue, T. Ohbayashi, M. Hirai, K. Noda, L.Y. Marmorstein, D. Yabe, K. Takagi, T.O. Akama, T. Kita, T. Kimura, T. Nakamura, Fibulin-4 conducts proper elastogenesis via interaction with cross-linking enzyme lysyl oxidase, Proc. Natl. Acad. Sci. U. S. A. 106 (45) (2009) 19029–19034.
[17] V. Hucthagowder, N. Sausgruber, K.H. Kim, B. Angle, L.Y. Marmorstein, Z. Urban, Fibulin-4: a novel gene for an autosomal recessive cutis laxa syndrome, Am. J. Hum. Genet. 78 (6) (2006) 1075–1080.
[18] M. Dasouki, D. Markova, R. Garola, T. Sasaki, N.L. Charbonneau, L.Y. Sakai, M.L. Chu, Compound heterozygous mutations in fibulin-4 causing neonatal lethal pulmonary artery occlusion, aortic aneurysm, arachnodactyly, and mild cutis laxa, Am. J. Med. Genet. A 143A (22) (2007) 2635–2641.
[19] J. Hoyer, C. Kraus, G. Hammersen, J.P. Geppert, A. Rauch, Lethal cutis laxa with contractural arachnodactyly, overgrowth and soft tissue bleeding due to a novel homozygous fibulin-4 gene mutation, Clin. Genet. 76 (3) (2009) 276–281.
[20] M. Renard, T. Holm, R. Veith, B.L. Callewaert, L.C. Ades, O. Baspinar, A. Pickart, M. Dasouki, J. Hoyer, A. Rauch, P. Trapane, M.G. Earing, P.J. Coucke, L.Y. Sakai, H.C. Dietz, A.M. De Paepe, B.L. Loeys, Altered TGFbeta signaling and cardiovascular manifestations in patients with autosomal recessive cutis laxa type I caused by fibulin-4 deficiency, Eur. J. Hum. Genet. 18 (8) (2010) 895–901.

[21] P.J. McLaughlin, Q. Chen, M. Horiguchi, B.C. Starcher, J.B. Stanton, T.J. Broekelmann, A.D. Marmorstein, B. McKay, R. Mecham, T. Nakamura, L.Y. Marmorstein, Targeted disruption of fibulin-4 abolishes elastogenesis and causes perinatal lethality in mice, Mol. Cell. Biol. 26 (5) (2006) 1700–1709.
[22] K. Hanada, M. Vermeij, G.A. Garinis, M.C. de Waard, M.G. Kunen, L. Myers, A. Maas, D.J. Duncker, C. Meijers, H.C. Dietz, R. Kanaar, J. Essers, Perturbations of vascular homeostasis and aortic valve abnormalities in fibulin-4 deficient mice, Circ. Res. 100 (5) (2007) 738–746.
[23] N.W. Ramnath, L.J. Hawinkels, P.M. van Heijningen, L. te Riet, M. Paauwe, M. Vermeij, A.H. Danser, R. Kanaar, P. ten Dijke, J. Essers, Fibulin-4 deficiency increases TGF-beta signalling in aortic smooth muscle cells due to elevated TGF-beta2 levels, Sci. Rep. 5 (2015) 16872.
[24] J. Huang, E.C. Davis, S.L. Chapman, M. Budatha, L.Y. Marmorstein, R.A. Word, H. Yanagisawa, Fibulin-4 deficiency results in ascending aortic aneurysms: a potential link between abnormal smooth muscle cell phenotype and aneurysm progression, Circ. Res. 106 (3) (2010) 583–592.
[25] D. Proudfoot, C. Shanahan, Human vascular smooth muscle cell culture, Methods Mol. Biol. 806 (2012) 251–263.
[26] O.H. Lowry, N.J. Rosebrough, A.L. Farr, R.J. Randall, Protein measurement with the Folin phenol reagent, J. Biol. Chem. 193 (1) (1951) 265–275.
[27] J. Schindelin, I. Arganda-Carreras, E. Frise, V. Kaynig, M. Longair, T. Pietzsch, S. Preibisch, C. Rueden, S. Saalfeld, B. Schmid, J.Y. Tinevez, D.J. White, V. Hartenstein, K. Eliceiri, P. Tomancak, A. Cardona, Fiji: an open-source platform for biological-image analysis, Nat. Methods 9 (7) (2012) 676–682.
[28] E. Meijering, O. Dzyubachyk, I. Smal, Methods for cell and particle tracking, Methods Enzymol. 504 (2012) 183–200.
[29] S. Dennler, S. Itoh, D. Vivien, P. ten Dijke, S. Huet, J.M. Gauthier, Direct binding of Smad3 and Smad4 to critical TGF beta-inducible elements in the promoter of human plasminogen activator inhibitor-type 1 gene, EMBO J. 17 (11) (1998) 3091–3100.
[30] X. Chen, R. Prywes, Serum-induced expression of the cdc25A gene by relief of E2F-mediated repression, Mol. Cell. Biol. 19 (7) (1999) 4695–4702.
[31] Y. Yamashiro, C.L. Papke, J. Kim, L.J. Ringuette, Q.J. Zhang, Z.P. Liu, H. Mirzaei, J.E. Wagenseil, E.C. Davis, H. Yanagisawa, Abnormal mechanosensing and cofilin activation promote the progression of ascending aortic aneurysms in mice, Sci. Signal. 8 (399) (2015) ra105.
[32] R.K. Prinjha, C.E. Shapland, J.J. Hsuan, N.F. Totty, I.J. Mason, D. Lawson, Cloning and sequencing of cDNAs encoding the actin cross-linking protein transgelin defines a new family of actin-associated proteins, Cell Motil. Cytoskeleton 28 (3) (1994) 243–255.
[33] P.J. Adam, C.P. Regan, M.B. Hautmann, G.K. Owens, Positive- and negative-acting Kruppel-like transcription factors bind a transforming growth factor beta control element required for expression of the smooth muscle cell differentiation marker SM22alpha in vivo, J. Biol. Chem. 275 (48) (2000) 37798–37806.
[34] T.D. Arnold, K. Zang, A. Vallejo-Illarramendi, Deletion of integrin-linked kinase from neural crest cells in mice results in aortic aneurysms and embryonic lethality, Dis. Model. Mech. 6 (5) (2013) 1205–1212.
[35] M.B. Hautmann, C.S. Madsen, G.K. Owens, A transforming growth factor beta (TGFbeta) control element drives TGFbeta-induced stimulation of smooth muscle alpha-actin gene expression in concert with two CArG elements, J. Biol. Chem. 272 (16) (1997) 10948–10956.
[36] Y. Liu, S. Sinha, G. Owens, A transforming growth factor-beta control element required for SM alpha-actin expression in vivo also partially mediates GKLF-dependent transcriptional repression, J. Biol. Chem. 278 (48) (2003) 48004–48011.
[37] R.J. Pelham Jr., Y. Wang, Cell locomotion and focal adhesions are regulated by substrate flexibility, Proc. Natl. Acad. Sci. U. S. A. 94 (25) (1997) 13661–13665.
[38] F.J. Byfield, R.K. Reen, T.P. Shentu, I. Levitan, K.J. Gooch, Endothelial actin and cell stiffness is modulated by substrate stiffness in 2D and 3D, J. Biomech. 42 (8) (2009) 1114–1119.
[39] N.L. Halliday, J.J. Tomasek, Mechanical properties of the extracellular matrix influence fibronectin fibril assembly in vitro, Exp. Cell Res. 217 (1) (1995) 109–117.
[40] J.R. Cook, N.P. Clayton, L. Carta, J. Galatioto, E. Chiu, S. Smaldone, C.A. Nelson, S.H. Cheng, B.M. Wentworth, F. Ramirez, Dimorphic effects of transforming growth factor-beta signaling during aortic aneurysm progression in mice suggest a combinatorial therapy for Marfan syndrome, Arterioscler. Thromb. Vasc. Biol. 35 (4) (2015) 911–917.
[41] W. Li, Q. Li, Y. Jiao, L. Qin, R. Ali, J. Zhou, J. Ferruzzi, R.W. Kim, A. Geirsson, H.C. Dietz, S. Offermanns, J.D. Humphrey, G. Tellides, Tgfbr2 disruption in postnatal smooth muscle impairs aortic wall homeostasis, J. Clin. Invest. 124 (2) (2014) 755–767.
[42] D.M. Milewicz, K.M. Trybus, D.C. Guo, H.L. Sweeney, E. Regalado, K. Kamm, J.T. Stull, Altered smooth muscle cell force generation as a driver of thoracic aortic aneurysms and dissections, Arterioscler. Thromb. Vasc. Biol. 37 (1) (2017) 26–34.
[43] S. Chen, R.J. Lechleider, Transforming growth factor-beta-induced differentiation of smooth muscle from a neural crest stem cell line, Circ. Res. 94 (9) (2004) 1195–1202.
[44] R. Morishita, K. Nagata, H. Ito, H. Ueda, M. Asano, H. Shinohara, K. Kato, T. Asano, Expression of smooth muscle cell-specific proteins in neural progenitor cells induced by agonists of G protein-coupled receptors and transforming growth factor-beta, J. Neurochem. 101 (4) (2007) 1031–1040.
[45] N.M. Shah, A.K. Groves, D.J. Anderson, Alternative neural crest cell fates are instructively promoted by TGFbeta superfamily members, Cell 85 (3) (1996) 331–343.
[46] S. Chen, M. Kulik, R.J. Lechleider, Smad proteins regulate transcriptional induction of the SM22alpha gene by TGF-beta, Nucleic Acids Res. 31 (4) (2003) 1302–1310.
[47] S. Chen, M. Crawford, R.M. Day, V.R. Briones, J.E. Leader, P.A. Jose, R.J. Lechleider, RhoA modulates Smad signaling during transforming growth factor-beta-induced smooth muscle differentiation, J. Biol. Chem. 281 (3) (2006) 1765–1770.
[48] I. Bultmann-Mellin, A. Conradi, A.C. Maul, K. Dinger, F. Wempe, A.P. Wohl, T. Imhof, F.T. Wunderlich, A.C. Bunck, T. Nakamura, K. Koli, W. Bloch, A. Ghanem, A. Heinz, H. von Melchner, G. Sengle, A. Sterner-Kock, Modeling autosomal recessive cutis laxa type 1C in mice reveals distinct functions for Ltbp-4 isoforms, Dis. Model. Mech. 8 (4) (2015) 403–415.
[49] I. Bultmann-Mellin, J. Essers, P.M. van Heijingen, H. von Melchner, G. Sengle, A. Sterner-Kock, Function of Ltbp-4L and fibulin-4 in survival and elastogenesis in mice, Dis. Model. Mech. 9 (11) (2016) 1367–1374.
[50] I. van der Pluijm, J. Burger, P.M. van Heijningen, I.J.A.N. van Vliet, C. Milanese, K. Schoonderwoerd, W. Sluiter, L.J. Ringuette, D.H.W. Dekkers, I. Que, E.L. Kaijzel, L. Te Riet, E. MacFarlane, D. Das, R. van der Linden, M. Vermeij, J.A. Demmers, P.G. Mastroberardino, E.C. Davis, H. Yanagisawa, H. Dietz, R. Kanaar, J. Essers, Decreased mitochondrial respiration in aneurysmal aortas of fibulin-4 mutant mice is linked to PGC1A regulation, Cardiovasc. Res. 114 (13) (2018 Nov 1) 1776–1793, https://doi.org/10.1093/cvr/cvy150 (PMID 29931197).
[51] T. Massam-Wu, M. Chiu, R. Choudhury, S.S. Chaudhry, A.K. Baldwin, A. McGovern, C. Baldock, C.A. Shuttleworth, C.M. Kielty, Assembly of fibrillin microfibrils governs extracellular deposition of latent TGF beta, J. Cell Sci. 123 (2010) 3006–3018 Pt 17.
[52] G. Gallo, Myosin II activity is required for severing-induced axon retraction in vitro, Exp. Neurol. 189 (1) (2004) 112–121.
[53] T. Mseka, L.P. Cramer, Actin depolymerization-based force retracts the cell rear in polarizing and migrating cells, Curr. Biol. 21 (24) (2011) 2085–2091.
[54] S.S. Rensen, P.A. Doevendans, G.J. van Eys, Regulation and characteristics of vascular smooth muscle cell phenotypic diversity, Neth. Heart J. 15 (3) (2007) 100–108.